HYDROLOGICAL PROCESSES
Hydrol. Process. **16**, 313–332 (2002)
DOI: 10.1002/hyp.337

Impact on Sahelian runoff of stochastic and elevation-induced spatial distributions of soil parameters

Luc Séguis,[1]* Bernard Cappelaere,[1] Christophe Peugeot[1] and Baxter Vieux[2]

[1] *U.M.R. Hydrosciences, Institut de Recherche pour le Développement (IRD, ex-ORSTOM), B.P. 5045, 34032 Montpellier Cedex 1, France*
[2] *School of Civil Engineering and Environmental Science, University of Oklahoma, Norman, OK 73019, USA*

Abstract:

Topography controls surface flows, and thereby exerts a significant action on soil formation. At the hillslope scale, infiltrability of the surface horizon varies gradually along the slope. In semi-arid zones, and especially in the Sahel, runoff is Hortonian and depends mainly on the hydraulic properties of the soil surface horizon (saturated hydraulic conductivity K_s and hydraulic roughness of the soil surface n). Using the fully distributed hydrologic model *r.water.fea* as an experimentation tool, this paper investigates the effects of various spatial distributions of K_s (deterministic, stochastic or a combination of both, all with an invariant global mean) and related n (taken as fully correlated to K_s) on the outflow of a small catchment representative of Sahelian conditions. In addition to a uniform distribution used as reference, deterministic distributions here consist of linear variations of K_s with elevation. A stochastic component is then added by drawing from a log-normal distribution with different variation coefficients C_v. Both hypothetical and real rainstorm events are tested.

All K_s distributions studied produce hydrographs that are very close to the uniform K_s case when rainfall is long and intense. For most other rain events, runoff increases with K_s variability. Whatever the rainfall event and C_v, outflow is greater when the less infiltrative surfaces are located downhill. The ratio of deterministic to purely stochastic variation is a good indication of the relative importance of the two K_s variation sources for catchment runoff. Given the high local-scale (stochastic) soil variability typically encountered, only strong catchment-scale contrasts really deserve to be included in the K_s distribution for runoff modelling of all but insignificant events. Spatial K_s representation can be further simplified down to a uniform distribution, when only a seasonal water yield is the required result. Copyright © 2002 John Wiley & Sons, Ltd.

KEY WORDS spatial variability; hydraulic conductivity; roughness; Hortonian runoff; Sahel; distributed modelling; stochastic hydrology

INTRODUCTION

Background

Topography, even with gentle slopes, exerts a significant action on soil formation through the fluxes (water, dissolved substances or particles) it controls. On a typical hillslope (stable slopes and homogeneous vegetation), soil characteristics generally vary gradually along the slope, whereas they exhibit little differences at equal elevations (Duchaufour, 1984; Loague and Gander, 1990). The concept of catena describes the spatial organization of soil types along the hillslope. Mechanical erosion dominates the hillslope tops, particles are detached and then carried downward. Consequently, a gradual clay enrichment of the surface horizon is observed along the slope, at the hillslope scale (Serpantié *et al.*, 1992). This results in a decrease in intrinsic infiltrability in lower areas. However, soil texture is only one amongst many factors controlling the infiltration capacity and its spatial variability. For instance, biological activity, vegetation cover, species and density also play important roles (Albergel *et al.*, 1986). Tillage and other soil practices, or vegetation growth, enhance

* Correspondence to: L. Séguis, U.M.R. Hydrosciences, Institut de Recherche pour le Développement (IRD, ex-ORSTOM), B.P. 5045, 34032 Montpellier Cedex 1, France. E-mail: seguis@mpl.ird.fr

Received 20 July 2000
Accepted 25 March 2001

infiltration. The general trend of infiltrability increase with elevation can thus be altered and even reversed by the action of man and vegetation.

In western Niger, a typical semi-arid region of the African Sahel, the main landscape features observed along a catena are the laterite-capped plateau, the sandy hillslope and the valley bottom; the infiltration capacity is typically higher in upslope areas. Owing to heavy rainstorms and poorly structured soils, soil surface crusts are commonly encountered, as in other Sahelian regions. As described by Hoogmoed and Strosnijder (1984) and Casenave and Valentin (1992), soil crusting plays a major role in the hydrology of these regions by locally reducing the infiltration capacity. Moving millet cultivation produces variations in hydraulic conductivity and surface roughness over time and space, due to crust destruction by tillage and subsequent crust restoration under rainfall (Peugeot *et al*., 1997). Hence, in modelling studies at the watershed scale, the slopewise-deterministic distribution of infiltration capacity induced by pedological processes must be considered together with a stochastic component due to the intrinsic small-scale spatial variability inherent to soil characteristics, and to time-dependent land use factors.

In semi-arid regions, runoff is generally Hortonian: overland flow occurs when the rainfall rate is greater than the saturated hydraulic conductivity K_s of the surface layer. Many studies have already focused on the influence of the spatial variability of infiltration on Hortonian runoff (e.g. Smith and Hebbert, 1979; Freeze, 1980; Woolhiser and Goodrich, 1988). Using mathematical modelling, these authors analysed the influence on runoff of a stochastic spatial distribution of K_s over a sloping plane. More precisely, Smith and Hebbert (1979) compared outflows produced by a random distribution of the conductivity with those resulting from a uniform distribution. They were found to differ significantly only when the rainfall intensity is low with regard to the hydraulic conductivity. Using a stochastic-conceptual model and Monte Carlo simulation, Freeze (1980) ranked as follows the K_s distribution parameters in decreasing order of importance for runoff: mean value, standard deviation and space autocorrelation function. He also showed that replacing a heterogeneous hillslope (variable K_s) by an 'equivalent' homogeneous hillslope (uniform K_s taken as the mean of the original distribution) can induce a significant bias in predicted runoff. To match the case of an actual watershed, Woolhiser and Goodrich (1988) introduced an impermeable channel reach at the downslope edge of the sloping plane. They showed that the channel had little influence on runoff at the outlet, compared with the infiltration characteristics over the plane. The hillslope they used consisted of five geometrically similar cascading panels, each of them being assigned a distinct K_s value drawn from a log-normal distribution. A comparison was made of outflows produced by this system and by a sloping plane with a uniform K_s, equal to the geometric mean of the panels' conductivities. The uniform hillslope was found to produce a higher peak discharge than did the heterogeneous hillslope when K_s was much lower than the average rainfall intensity. On the other hand, storms of short duration and high K_s values led to a higher discharge from the heterogeneous hillslope. More recently, but still for a sloping plane, Corradini *et al*. (1998) pointed out the importance of considering the 'run-on' effect, which augments the rainfall at any point of the catchment with the overland flow from upstream areas, giving this flow opportunities for infiltration in permeable downstream areas. They found that ignoring run-on induces an overestimation of the flow in the rising and recession limbs of the simulated hydrographs. Bearing in mind that Freeze's (1980) model did not take into account the run-on process, his conclusions should be kept in perspective. Besides, the conclusions of all these studies were obtained on sloping planes with rectilinear parallel flow-paths, and may become false on actual watersheds where topography induces flow concentration, i.e. the convergence of water flow-paths. Furthermore, these studies considered only a limited range of storm and infiltration characteristics.

More systematic was the study carried out by Saghafian *et al*. (1995), on a real watershed's geometry and topography with a broad range of rainfall intensities and conductivities. Using a two-dimensional distributed rainfall-runoff model, they compared the runoff discharges and volumes obtained for a log-normal distribution of K_s and for a uniform K_s value equal to the mean value of the log-normal distribution respectively. They mainly pointed out that the use of an average K_s value over the catchment generally tends to underestimate the runoff volume and the peak discharge at the outlet. It should be noted that, owing to the basin's surface area ($32{\cdot}2\ km^2$), the grid size was deliberately large (600 m) to reduce computation time, thereby underestimating the convergence of hillslope flow. When assigning the hydraulic conductivity values, no distinction was made between the drainage network and the rest of the catchment.

The previous authors considered only the influence of a purely stochastic K_s variability at the hillslope or watershed scale. As already mentioned, the variability of infiltration generally has a slopewise-deterministic component related to the location within the catena. Several authors (Smith and Hebbert, 1979; Hawkins and Cundy, 1987; Woolhiser *et al.*, 1996) have found that computed hillslope runoff is smaller when K_s increases downwards than when it decreases downwards. However, these analyses were performed for plane hillslopes only.

In the above cited studies, hydraulic roughness of the soil surface was considered uniform.

Objectives

The purpose of this paper is to investigate, through simulation with a distributed hydrological model, the effects on catchment runoff of combined stochastic and slopewise-deterministic variability of soil hydraulic parameters. Ultimately, these investigations should provide information about possible simplifications of soil hydraulic variability representation in distributed or semi-distributed models for small-size catchments. The analysis is performed for Hortonian runoff, the prevailing surface flow generation process in semi-arid areas. The topography, rainfall data, and available soil information for a small catchment in western Niger (Africa) are used for this purpose. The objective here is not to model the specific behaviour of this particular catchment, but to use the information on order of magnitude of different variables that is contained in the data, in order to set the framework for our simulation analyses, and ensure that these are both realistic and of general interest.

The soil parameters considered are the saturated hydraulic conductivity of the upper horizon K_s and the Manning roughness n, which have been shown respectively by Vandervaere *et al.* (1998) and Peugeot (1995) to be key factors for runoff in the Sahelian region. In this region, hydraulic conductivity and roughness are essentially controlled by the so-called surface features (Casenave and Valentin, 1992) that integrate the effects of soil crusting, vegetation and biological and human activities. As shown later in this paper, this makes the two parameters closely correlated, allowing the latter to be considered as directly dependent on the former.

The complexity of the spatial distribution of K_s is gradually increased: K_s is first taken as uniform over the catchment, then a strictly slopewise-deterministic distribution is used, to which a stochastic component is finally added. Though initially no distinction is made in the conductivity distributions between hillslopes and channel reaches, the effect of a higher K_s in the drainage network is investigated in the last part of the paper, to represent the commonly higher infiltration capacities of dryland channels.

Rainfall is first input to the model as a hypothetical rectangular hyetograph defined by a duration and a constant intensity, then as actual hyetographs observed in western Niger. Owing to the small catchment size, rainfall is assumed to be spatially uniform.

MATERIALS AND METHODOLOGY

The hydrologic model

All simulations are performed with the physically based, two-dimensional (2D), distributed model *r.water.fea* (Vieux and Gaur, 1994), which runs in the GRASS GIS environment (Westervelt, 1991) over a raster grid. Maps of the watershed geometry (catchment and channel network layout, rasterized drainage directions) produced from a digital elevation model (DEM) by GRASS's *r.watershed* function (USACE, 1993), define the discrete model structure.

On each grid cell, the overland and channel flows are described by the kinematic-wave approximation of De Saint–Venant equations:

$$\frac{\partial h}{\partial t} + \frac{\partial q}{\partial x} = r - f \tag{1}$$

where h is the water depth over the soil surface [L], q the surface flow rate (flow velocity u times flow depth h) [L^2T^{-1}], r the rainfall rate [LT^{-1}], f the infiltration rate [LT^{-1}], t is time [T], and x is the space dimension in the direction of slope [L].

The Green–Ampt equation is used to calculate the infiltration rate as:

$$f = K_s \left[1 + \frac{(H_f + h)\,\Delta\Theta}{F} \right] \tag{2}$$

where K_s is the saturated hydraulic conductivity [LT^{-1}], H_f the capillary pressure head at the wetting front [L], $\Delta\Theta$ the initial soil water deficit, and F the cumulated infiltrated depth since the beginning of the rainfall event [L].

The equation system is closed with the Manning resistance equation relating the flow velocity u [LT^{-1}] and the hydraulic radius R[L]:

$$u = \frac{1}{n} R^{2/3} S^{1/2} \tag{3}$$

with n the Manning coefficient of hydraulic roughness [$L^{-1/3}T$] and S the land slope. For overland flow, R can be approximated by the water depth h.

The above infiltration and surface flow formulations are fully coupled by concurrent solving within the partial differential Equation (1) using a finite-element method in space and an explicit finite-difference scheme over time. Each node of the 2D raster grid is connected by a linear finite-element to its downstream neighbour node. Hence, the finite-element topology is derived from the 2D drainage structure input map. The continuity at each element node ensures at any time that the runoff flow rates from connecting upstream elements are accounted for as the run-on flow rates into the collecting element for that node.

The model parameters (saturated conductivity, capillary pressure head at the wetting front, Manning coefficient) and the slope are handled as GRASS raster maps. Although *r.water.fea* may be run with distributed rainfall maps, only spatially uniform rainfall is considered here. The model is operated on an event basis: an initial soil moisture map is input to the model, which will here be taken as uniform over the catchment for the purposes of the present simulation analyses, as explained below.

The watershed

In this section, we present the topography and the K_s variability observed in the small Sahelian catchment of Wankama (1·875 km^2), which will be used as our prototype catchment. The watershed is located north-east of Niamey (Niger, West Africa), where the Hapex–Sahel experiment was conducted from 1992 to 1994 (Goutorbe *et al*., 1994). Rainstorms occur between May and September, with a mean annual rainfall depth of 560 mm (Le Barbé and Lebel, 1997). The landscape, of gentle topography, is organized by laterite plateaux that delimit wide, sandy, generally extensively cultivated valleys. Storm water flowing down the plateau edges reaches sand-blocked fossil valley bottoms where it accumulates into small pools and subsequently recharges the underlying aquifer. This hydrographic feature, called endoreism, is ubiquitous in this region: it is induced by gentle slopes, aeolian sand deposits and the small annual number of rainfall events. The Wankama basin is representative of the area with a 2% mean slope and crust-prone, sandy soils. The stream network consists of a deep, sandy-bed single gully (Figure 1), with high infiltration capacity.

The water table being approximately 30 m below the lowest locations of the watershed, ground water does not act on runoff, which is exclusively Hortonian overland flow. Local-scale infiltration is mainly driven by the soil surface characteristics. Casenave and Valentin (1992) developed the concept of 'soil surface features' to characterize the infiltration/runoff properties of the various types of soil surface encountered in the Sahel region. Based upon rainfall simulation data for 87 plots in the region, they built a classification of the various soil surface conditions encountered, using as criteria the key factors in terms of hydrological behaviour: surface crust type, faunal activity (e.g. termites), woody and herbaceous vegetation cover, surface roughness.

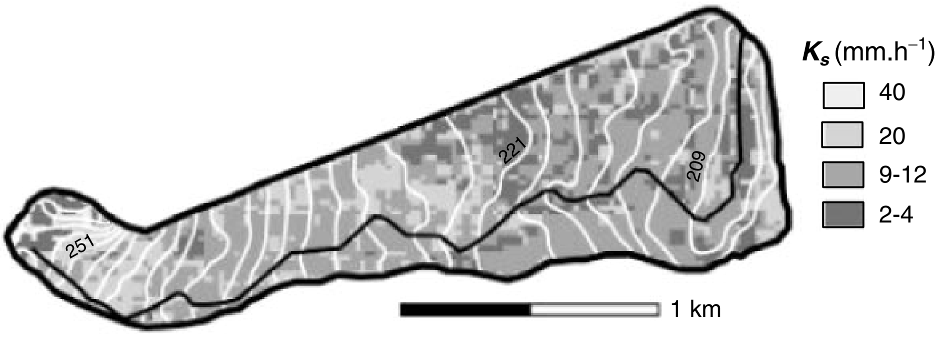

Figure 1. Topography and saturated hydraulic conductivity K_s of Wankama watershed (Niger)

Soil surface feature units can be mapped from field survey (Valentin, 1986) or from remote sensing image analysis (Lamachère and Puech, 1996). Casenave and Valentin's (1992) classification associates to each soil surface feature class an estimate of the infiltration rate derived from the rainfall simulation experiments. These estimates are consistent with direct measurements of saturated hydraulic conductivity (Valentin, 1991; Peugeot *et al*., 1997; Vandervaere *et al*., 1997).

D'Herbès and Valentin (1997) produced a soil surface feature map for the Niamey area containing the Wankama catchment, by classification of SPOT multi-spectral images at a 20 m resolution together with transects obtained from field survey. Using Casenave and Valentin's table of surface features and hydrological characteristics (Table I), a 20 m resolution K_s map was derived (Figure 1). Desconnets *et al*. (1996) added to this table estimates of the Manning roughness parameter n for the surface feature classes encountered in the Niamey area (Table I), and obtained a 20 m resolution hydraulic roughness map. They produced a DEM from a 1/5000 topographical field survey with a 20 m resolution in space and 10^{-2} m in elevation. The 20 m resolution is used here for all our hydrological simulation analyses.

The relationship between elevation z and K_s is derived by cross-tabulating the two mapped variables. Circles in Figure 2 give the mean K_s value calculated for each 1 m elevation class. These values grow from

Table I. Characteristics of land surface types encountered over the Wankama catchment; after D'Herbès and Valentin (1997) and Desconnets *et al*. (1996)

Land surface condition	Main soil crust[a]	Herbaceous cover (%)	K_s (mm h^{-1})	Hydraulic roughness n
Plateau: bare soil	Gravel	0	2	0·020
Plateau: dense vegetation	No	<10	40	0·250
Hillslope iron pan	Erosion	<15	3	0·046
Degraded hillslope	Erosion	<5	4	0·015
Hillslope low density field	Structural	15–25	13	0·143
Hillslope high density field	Structural	25–35	13	0·100
Valley bottom low density field	Erosion	15–25	9	0·167
Valley bottom high density field	Structural	25–50	13	0·125
Old dense shrub fallow	Drying	25–50	13	0·125
Old mid-dense shrub fallow	Drying	50–75	20	0·167
Old sparse shrub fallow	Drying	>75	20	0·200
Mid-old high grass fallow	Drying	50–75	20	0·167
Mid-old low grass fallow	Drying	<50	20	0·143
Recent fallow	Drying	50–75	20	0·143

[a] Terminology by Casenave and Valentin (1992).

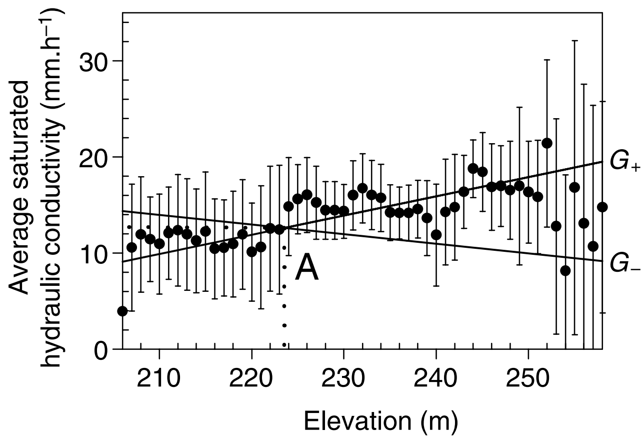

Figure 2. Mean saturated hydraulic conductivity (with plus/minus one standard deviation) per 1 m elevation class and linear $K_s(z)$ relationships used in simulations (G_+, G_-)

4 mm h^{-1} at the bottom of the catchment ($z = 208$ m) up to 22 mm h^{-1} for the 251 m elevation. The areas above this altitude are flat tiger bush plateaux with minute slope. Tiger bush is characterized by a banded pattern of dense vegetation patches with high infiltration capacity alternating with runoff-producing bare zones. This alternation explains the large variability of K_s for elevations above 251 m. In actual fact, the overall plateau contribution to catchment runoff is very low due to quasi-total abstraction of bare soil runoff by the vegetation bands; it may therefore be ignored. Outside the plateau areas, the typical trend of downslope K_s decrease is observed.

Simulation protocol

This section describes the model-based experiment design used to explore the effect of soil variability on runoff. The generation of relevant samples of deterministic and/or stochastic K_s distributions and rainfall events is presented, successively.

Deterministic K_s component. Excluding plateau hydraulic conductivities, a linear relationship is applied between elevation and K_s (Figure 2):

- constrained by point A whose z and K_s coordinates (223·3 m and 12·6 mm h^{-1} respectively) are the global averages for the two mapped variables over the watershed;
- closely fitting the circles of Figure 2 beneath 251 m:

$$K_s(z) = 9{\cdot}0 + 0{\cdot}2(z - 205{\cdot}5) \qquad (r^2 = 0{\cdot}62) \tag{4}$$

where z (m) is the elevation and K_s (mm h^{-1}) the saturated hydraulic conductivity.

As mentioned in the Introduction, the reverse configuration, i.e. K_s decreasing with elevation, might also be encountered. Therefore, a second linear relationship is considered in which K_s decreases upslope as defined by the following points:

- the minimum K_s value is 9 mm h^{-1}, i.e. the same as in Equation (4), obtained this time for the maximum elevation $z = 260$ m;
- point A already defined.

This negative relationship reads:

$$K_s(z) = 14{\cdot}4 - 0{\cdot}1(z - 205{\cdot}5) \quad (5)$$

The two opposite gradient trends of Equations (4) and (5) are referred to as G_+ and G_- respectively. Constraining G_+ and G_- to point A preserves the overall average K_s value over the catchment: K_s maps computed from the DEM with Equations (4) and (5) have a mean of 12·6 mm h^{-1}, as the original map. Their variances are 7·18 mm^2 h^{-2} and 1·74 mm^2 h^{-2} for the G_+ and G_- distributions respectively.

Vegetation cover favourable to biological activity (worms, termites) enhances infiltration (Hino *et al.*, 1987; Séguis and Bader, 1997) and increases the surface roughness (Albergel *et al.*, 1986). Soil hydraulic conductivity and roughness are thus closely related. The cross-tabulation of the conductivity and hydraulic roughness raster maps of the Wankama watershed is illustrated in Figure 3 for the surface feature classes encountered in the catchment. It may be noticed that the effects on infiltration of K_s and n are cumulative: lower n, meaning shorter opportunity time for infiltration, occurs concurrently with lower K_s and, conversely, higher n with higher K_s.

The following exponential formulation is fitted to the plot:

$$\frac{1}{n} = 2 + 67{\cdot}03\ e^{-0{\cdot}15K_s} \quad (6)$$

Through this expression, the hydraulic roughness n is considered here as a dependent variable fully subjected to K_s.

With Equations (4) or (5), and (6), deterministically distributed hydraulic conductivity and roughness raster maps can be generated from the elevation map. A uniform distribution of $K_s = 12{\cdot}6$ mm h^{-1} over the basin is used as a third deterministic pattern in addition to the above G_+ and G_- linear distributions, and is referred to as the G_0 case. Each hydrological simulation requires both a set of conductivity and roughness raster maps and a rainfall hyetograph. All simulations are performed with a 5 s time step.

Stochastic K_s component. To account for the 'natural' small-scale variability of K_s, a stochastic component is added to the three above strictly deterministic evaluations of K_s. Within each elevation class, this stochastic component is assumed to belong to the same homogeneous population for that class. The type of K_s data available for the Niamey area (classified pixel values, with a small number of classes) does not allow for drawing more information about these populations than their first two moments (mean, standard deviation; see Figure 2). A log-normal distribution was chosen in accordance with a number of studies (Nielsen *et al.*, 1973; Anderson and Cassel, 1986; Boivin *et al.*, 1987), showing that hydraulic conductivity is log-normally distributed in space. For each grid cell of altitude z, K_s is drawn from a log-normal distribution for this z value with a mean equal to $K_s(z)$ [Equation (4) or (5), or 12·6 mm h^{-1}, for G_+, G_- or G_0 respectively] and a variation coefficient (variance-to-mean ratio) set as a parameter, C_v. A Manning roughness value is then

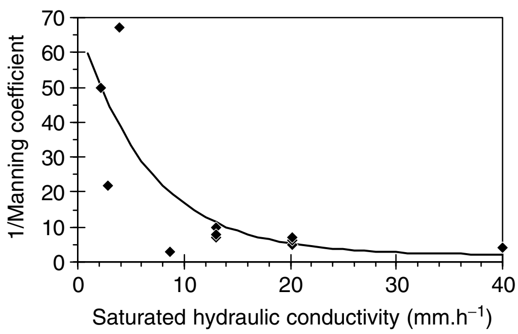

Figure 3. Manning roughness coefficient versus saturated hydraulic conductivity

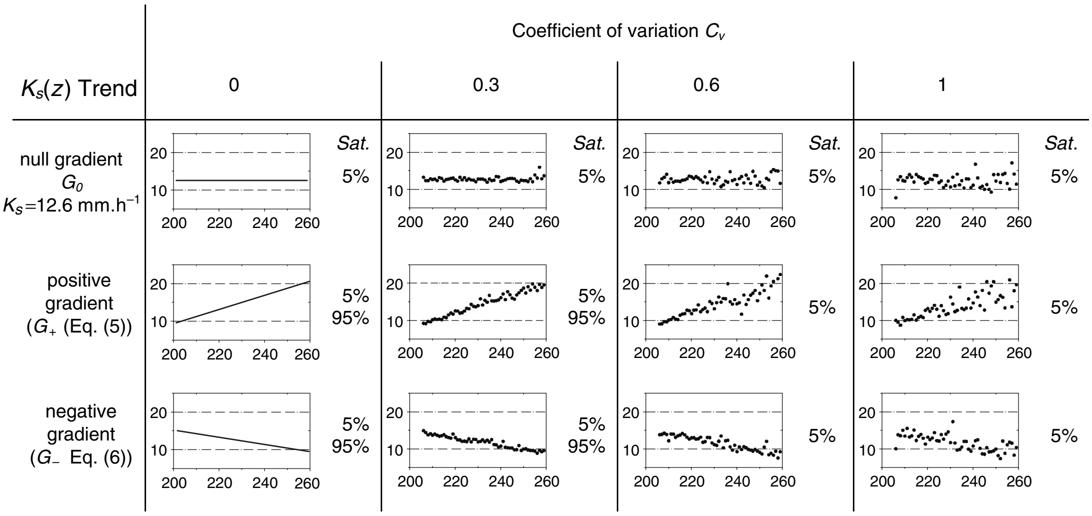

Figure 4. Simulation design with respect to $K_s(z)$ trend, coefficient of variation C_v and initial degree of saturation of the basin (*Sat.*). Each graph [elevation (m) on x-axis and K_s (mm h^{-1}) on y-axis] shows a simulated $K_s(z)$ distribution example

associated to this hydraulic conductivity value through Equation (6). No spatial correlation is included in the K_s stochastic distribution component because it is often considered as a term of lesser importance for runoff generation, after the mean value and the standard deviation of K_s (Freeze, 1980). Hence K_s correlation exists here in space only through the slopewise-deterministic component.

A Monte Carlo method is used to analyse the watershed responses to the stochastic and deterministic distributions of K_s. Fifty sets of conductivity and roughness maps were generated using the above method. Previous sensitivity analyses (Saghafian *et al.*, 1995; Corradini *et al.*, 1998) showed that 50 simulations are sufficient to encompass most of the runoff response variability due to the stochastic variation of K_s. The analysis focuses on the following outflow characteristics at the outlet, averaged over each set of 50 runs: initiation time, volume and peak discharge.

K_s raster maps and associated Manning's roughness maps are generated using C_v values of 0 (strictly deterministic distribution), 0·3, 0·6 and 1. These values are in the range of those described in the literature (Nielsen *et al.*, 1973; Vauclin, 1982; Woolhiser and Goodrich, 1988). Figure 4 summarizes the whole set of simulations carried out in the study. For the non-zero coefficients of variation, each plot of average K_s (mm h^{-1}, on y-axis) versus elevation class (m, on x-axis) is an example among 50 generated raster maps (note that the K_s averaging per z-class in Figure 4 produces a variability reduction, compared with C_v, which is dependent on the pixel number per class).

In a first step of the analysis, the K_s and n raster maps over the basin are generated with no special treatment for the channel network: for each network pixel, K_s is derived from elevation. In the second step, the river network (Figure 1) is explicitly defined by assigning a uniform K_s value of 150 mm h^{-1} and n of 0·03. These values are in accordance with published data for clean sandy dryland river beds (Chow, 1959; Rawls *et al.*, 1982).

Rainfall. The synthetic rainstorm set is built according to the method developed by Saghafian *et al.* (1995), and summarized below. Rainstorms are assumed spatially uniform over the small catchment, with constant intensity and variable duration. Each rainfall event is defined by two dimensionless parameters: K^* for intensity and T^* for duration. K^* is defined as:

$$K^* = \frac{K_s}{i} \tag{7}$$

where K_s is the mean saturated hydraulic conductivity of the basin, and i is the steady rainfall intensity [LT^{-1}]. Let us assume a uniform distribution of K_s (12·6 mm h^{-1}), and let t_p be the ponding time at which saturation occurs. The ponding time is calculated according to Mein and Larson (1973) by the equation:

$$t_p = \frac{K_s H_f \Delta\Theta}{i(i - K_s)} \tag{8}$$

Let t_e be defined as the steady-state time-to-equilibrium at the basin outlet: for a storm of intensity i and unlimited duration, t_e is the time lag between the beginning of the rainstorm and the beginning of steady-state discharge at the outlet for an impermeable basin. It depends on rainfall intensity and encompasses basin geometry and hydraulic roughness. Finally, let t_{re} be the sum of t_p and t_e : t_{re} is a characteristic time of the watershed for a given rainfall intensity and initial soil moisture. T^* is then defined as the ratio of rainstorm duration t_r to the characteristic time t_{re}:

$$T^* = \frac{t_r}{t_{re}} = \frac{t_r}{t_p + t_e} \tag{9}$$

These dimensionless parameters K^* and T^* are given the values shown in Table II, in the range 0·1 to 0·9 for K^* (eight values) and 0·05 to 2·0 for T^* (ten values). To compute rainfall intensities, the average value of 12·6 mm h^{-1} is used for K_s, whatever the $K_s(z)$ trend considered, leading to rainfall intensities in the range of 14 to 126 mm h^{-1} (always above the average K_s value of 12·6 mm h^{-1}).

The time-to-equilibrium t_e is computed for each of these rainstorms with the *r.water.fea* model for an impermeable basin. The steady state is considered to be reached when the outlet discharge variation between two successive time steps is lower than 10^{-3} m^3 s^{-1}. Hence, a set of 80 rainfall events is defined for each of two initial degrees of saturation (defined below), giving a total of 160 events. Table II shows the rainfall duration values for these synthetic rainstorms.

Other parameters. Most often the water content in the first few centimetres of Sahelian soils, which controls the infiltration/runoff process, is very low at the onset of a storm event (Cuenca *et al.*, 1997). This is due to the very fast drying under very high potential-evapotranspiration conditions, to the sandy texture of soils

Table II. Rainfall duration (minutes) versus T^*, K^* and initial degree of saturation

K^*		T^*									
		0·05	0·1	0·2	0·3	0·4	0·5	0·7	1	1·5	2
Sat.: 5%	0·1	2	4	7	11	15	18	26	37	55	74
	0·2	2	5	9	14	19	23	32	46	70	93
	0·3	3	5	11	16	22	27	38	55	82	109
	0·4	4	7	14	22	29	36	50	72	108	144
	0·5	4	9	18	27	36	45	63	90	135	180
	0·6	6	12	25	37	49	62	86	123	185	246
	0·8	14	28	57	85	113	142	198	283	425	566
	0·9	31	62	124	185	247	309	432	618	926	1235
Sat.: 95%	0·1	2	4	7	11	14	18	25	36	54	72
	0·2	2	4	9	13	17	22	30	43	65	86
	0·3	2	5	9	14	19	23	33	46	70	93
	0·4	3	5	11	16	22	27	38	55	82	110
	0·5	3	6	12	17	23	29	40	58	87	116
	0·6	3	7	13	20	26	33	46	65	98	130
	0·8	4	8	15	23	31	39	54	77	116	155
	0·9	5	10	19	29	39	48	68	97	145	194

and to generally long interstorm durations (Thauvin, 1992). Only when a second storm follows shortly after a first one within the same meteorological event (a rather infrequent occurrence in the area) can the initial soil moisture condition be significantly wetter. In our analyses, the initial degree of saturation $[1 - \frac{\Delta\Theta}{\Theta_s}$, where Θ_s is the porosity] will be taken equal to either 5%, to represent the usually dry condition, or 95% to account for a possible sequence of storms within a single meteorological event. For all simulations, a value of 5 cm will be taken for the capillary pressure head at the wetting front H_f.

RESULTS

The influence on catchment discharge of an increasing complexity in the spatial distribution of K_s (and associated n) is analysed in three steps, for an initial degree of saturation of 5%. The results obtained with a strictly deterministic distribution of K_s (G_+ or G_-) are first compared with those from a uniform K_s value (G_0). Then the streamflows resulting from the addition of a stochastic component with increasing variance are compared with those obtained with a uniform K_s distribution (G_0, $C_v = 0$). A drainage network with distinct parameters is then included. Finally, the influence of initial moisture is studied and simulations are performed with actual rainstorms and hydraulic parameters.

Strictly deterministic space distribution of hydraulic parameters

This is the case where C_v is null (first column of Figure 4). The 80 event simulations obtained for each of G_+ and G_- trends are compared with the 80 simulations obtained for the G_0 case (spatially uniform hydraulic parameters). Results, consisting of the discharge initiation time t_i, runoff volume V and peak discharge Q, are made dimensionless through division by the G_0-case values, i.e. (for the positive gradient G_+ example):

$$t_i^* = \frac{t_{i(G_+,C_v=0)}}{t_{i(G_0,C_v=0)}} \quad V^* = \frac{V_{(G_+,C_v=0)}}{V_{(G_0,C_v=0)}} \quad Q^* = \frac{Q_{(G_+,C_v=0)}}{Q_{(G_0,C_v=0)}} \tag{10}$$

Initiation time t_i^*. t_i^* versus K^* for the strictly deterministic case is shown on the two upper curves (square symbols) of Figure 5. For G_+ (dotted line), t_i^* is always lower than unity, meaning that the outflow initiation

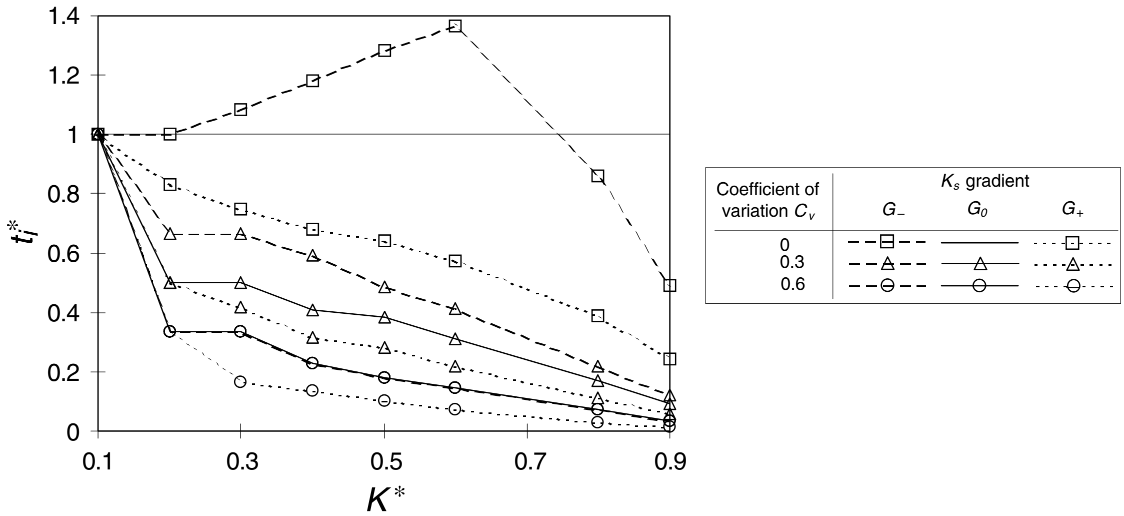

Figure 5. Dimensionless discharge initiation time t_i^* versus K^*, C_v and K_s gradient

time is always shorter than for G_0. This is due to the low K_s values near the outlet, compared with uniform K_s. For all rainfall intensities, the initiation time is controlled by the ponding time in the lower area of the catchment, leading to a decreasing t_i^* with increasing K^*, as may be inferred from Equation (8). The opposite happens for G_- (dashed line in Figure 5), except that as the lower area ponding time increases, the role of upper areas (K_s lower than mean) in outflow initiation gradually grows, as evidenced by the decreasing initiation time for higher K^*.

Outflow volume V^*. The two graphs of Figure 6 present, for G_- and G_+ respectively, the variation of the dimensionless outflow volume V^* for various rainstorms defined by (T^*, K^*). Both graphs show that V^* tends to unity when T^* increases or K^* decreases. This means that the effect of the spatial distribution of K_s increases when the rainstorm intensity and duration decrease (high K^* and low T^*), i.e. in conditions of lesser runoff.

For G_+, V^* is always higher than unity (all the more so as rain intensity and duration decrease), illustrating the fact that this spatial distribution of K_s produces more runoff than a uniform watershed. In the G_- case, some V^* values are lower than unity. They are associated with rainfall events of high to medium intensity ($0{\cdot}2 \le K^* \le 0{\cdot}5$) and short duration ($T^* \le 0{\cdot}5$), i.e. with rainstorms that produce only moderate runoff due to the duration factor. In such conditions, there is more possibility in the G_- case for run-on originating in upper, less permeable areas to infiltrate on the way down to the outlet, compared with the uniform case. Only when runoff is small due to the intensity factor (i.e. high K^*) will V^* show a value significantly higher than unity for G_-. Figure 6 also shows that the outflow volumes obtained with G_- are always smaller than those obtained with G_+, whatever the rainfall event characteristics.

The same type of analysis has been performed for the dimensionless peak discharge Q^*. The results, not presented here, show that Q^* behaves similarly to V^*.

Stochastic-deterministic space distribution of hydraulic conductivity and roughness

The total number of hydrological simulations carried out is 36 000, corresponding to the combination of three gradients (G_+, G_-, G_0), three coefficients of variation C_v (0·3, 0·6, 1), 50 stochastically generated raster maps of K_s and n and 80 storms.

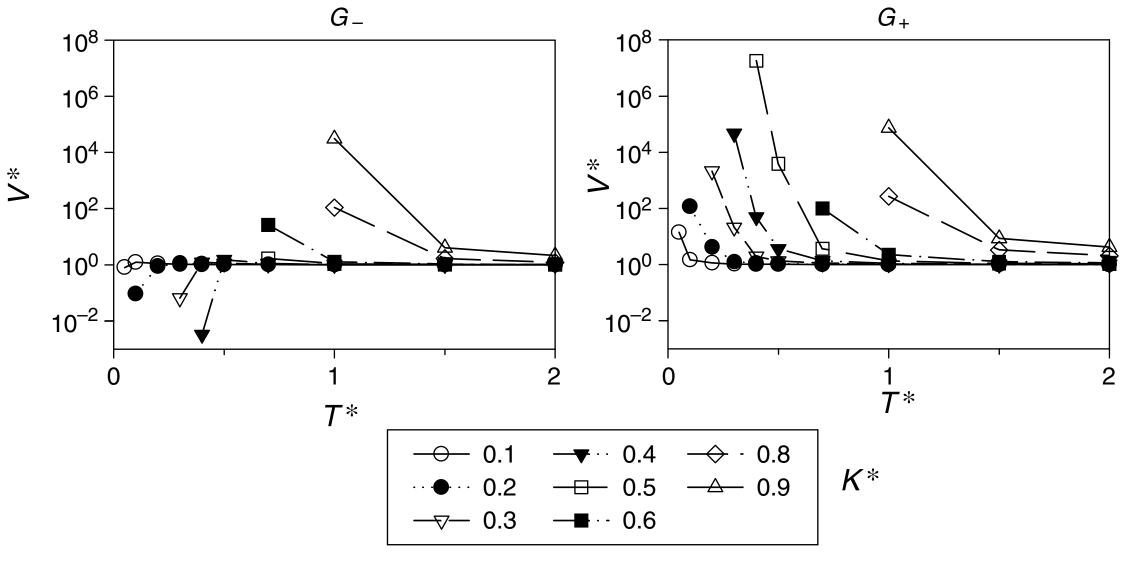

Figure 6. Dimensionless outflow volume V^* versus T^* and K^*, for deterministic K_s (G_- or G_+)

The simulation results are analysed through the dimensionless discharge initiation time, outflow volume and outlet peak discharge, now defined (taking G_+ as an example) as:

$$t_i^* = \frac{\overline{t}_{i(G_+,C_v\neq 0)}}{t_{i(G_0,C_v=0)}} \quad V^* = \frac{\overline{V}_{(G_+,C_v\neq 0)}}{V_{(G_0,C_v=0)}} \quad Q^* = \frac{\overline{Q}_{(G_+,C_v\neq 0)}}{Q_{(G_0,C_v=0)}} \tag{11}$$

where the upper bar in the numerators designates the averages over the 50 stochastic realizations for a particular parameter set [combination of gradient, C_v and storm (K^*, T^*)], the denominators being the same as in the previous section.

Initiation time t_i^*. The relationship between t_i^* and K^* for the three gradients and for three C_v values (0 to 0·6) is shown in Figure 5. When the K_s distribution includes a stochastic component ($C_v > 0$), t_i^* is lower than unity and decreases with increasing K^* whatever the gradient of K_s. A stochastic component always leads to the presence of some low K_s values (<12·6 mm h^{-1}) for some pixels near the outlet, even for G_-, producing a behaviour similar to the (G_+, $C_v = 0$) case with regard to initiation time. Increasing the coefficient of variation induces earlier runoff generation. For whatever C_v and K^* values, discharge initiation is delayed for a negative K_s gradient compared with a positive one.

Outflow volume V^*. Separately for the three deterministic K_s trends (G_-, G_0, G_+), Figure 7 presents the variations of the dimensionless outflow volume V^* for the three non-zero C_v values and for various rainstorms defined by (T^*, K^*). With any stochastic K_s component ($C_v \neq 0$), V^* is higher than unity whatever the K_s gradient and rainfall, in contrast to Figure 6 ($C_v = 0$, i.e. purely deterministic case) where values smaller than unity were observed for G_-. As in Figure 5, V^* tends to unity when T^* increases or K^* decreases (higher runoff conditions). This result previously described by Saghafian *et al.* (1995) for the purely stochastic case (G_0, $C_v \neq 0$) is confirmed in our study, with or without the deterministic component (G_- or G_+, $C_v \neq 0$): whatever the nature of the variability, deterministic and/or stochastic, the spatial variability of K_s has a higher impact when the rainfall event is short and/or of small intensity. For a null gradient, the introduction of

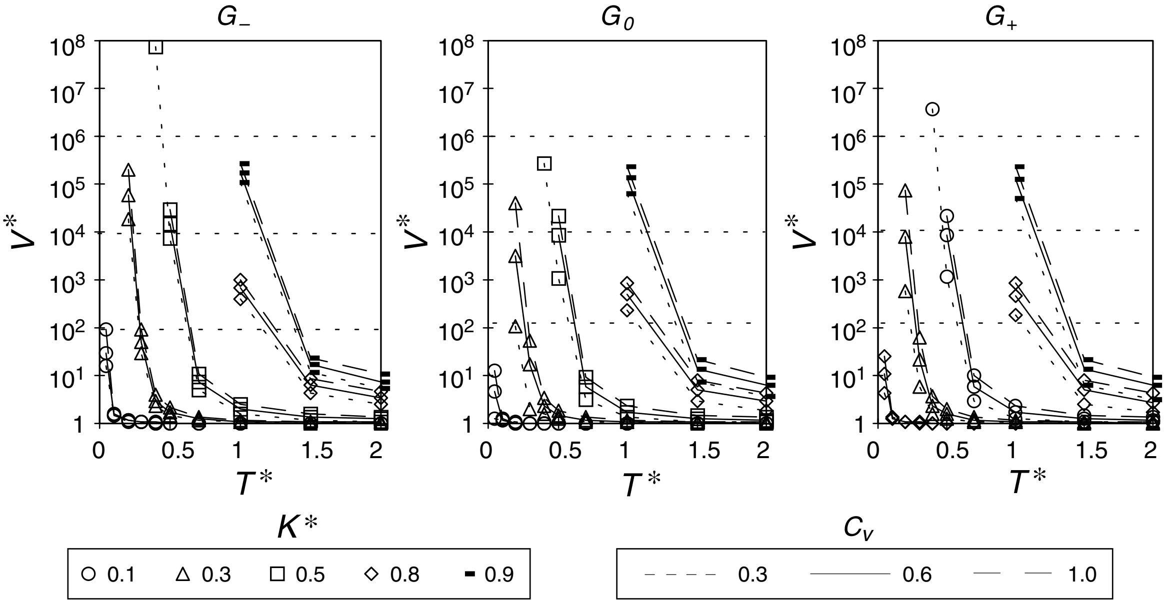

Figure 7. Dimensionless outflow volume V^* versus T^*, K^*, C_v and K_s gradient, for stochastic-deterministic K_s

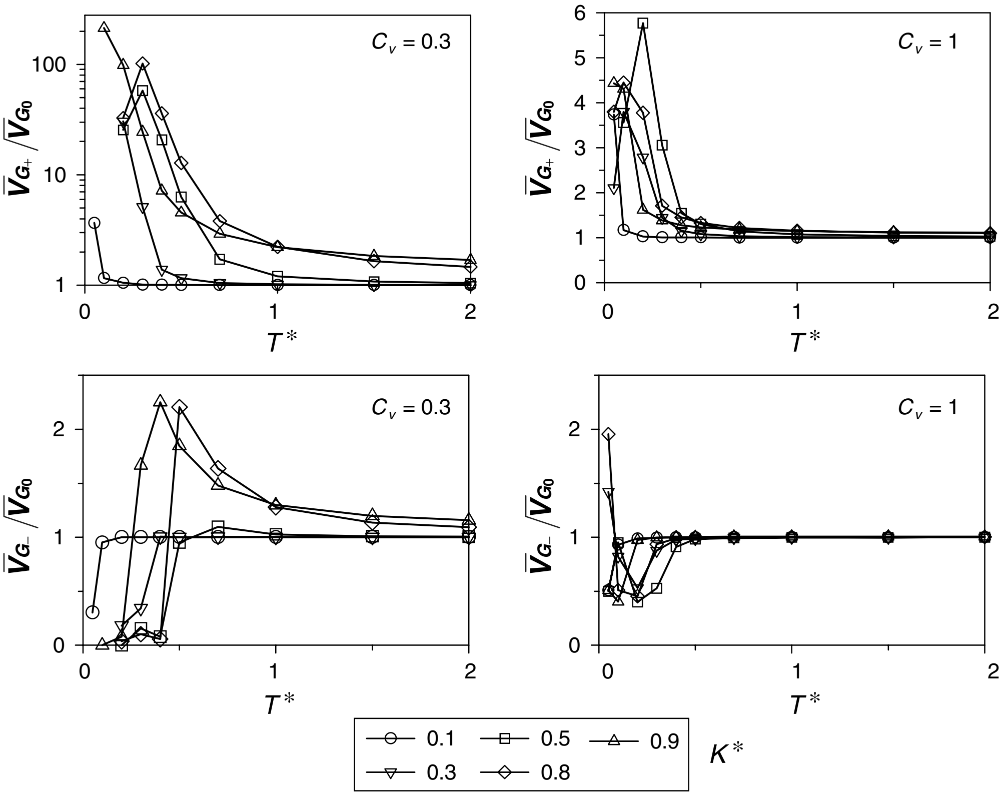

Figure 8. Ratio of outflow volume with K_s gradient ($\overline{V}_{G_+}$ or $\overline{V}_{G_-}$) to outflow volume without K_s gradient ($\overline{V}_{G_0}$), versus T^*, K^* and C_v

random space variability, even small ($C_v = 0{\cdot}3$), results in a very large increase in the outflow volume, for such 'favourable' events.

To measure the effect of the deterministic K_s gradient on simulated volumes for a given variation coefficient C_v, Figure 8 shows the ratios of outflow volumes (means over 50 runs) computed as:

$$\overline{V}_{G_+}/\overline{V}_{G_0} = \overline{V}_{(G_+,C_v)}/\overline{V}_{(G_0,C_v)} \text{ and } \overline{V}_{G_-}/\overline{V}_{G_0} = \overline{V}_{(G_-,C_v)}/\overline{V}_{(G_0,C_v)} \quad (12)$$

For a small variation coefficient ($C_v = 0{\cdot}3$), the results are consistent with those outlined in Figure 6 for $C_v = 0$: in the G_+ configuration they are always higher than unity, whereas for G_- the ratios are lower than unity for brief rainstorms, and higher than unity (although much less than in the $C_v = 0$ case) for longer rainstorms of low intensity. When the variation coefficient increases ($C_v = 1$), the runoff volumes produced with the positive or negative gradient are much closer to the runoff volumes obtained with a null gradient (ratios closer to unity). Hence, as a consequence of an increase in the variation coefficient, the spatial heterogeneity due to the stochastic component of K_s becomes predominant over the spatial variability introduced by the K_s gradient. Given a rainfall event and a variation coefficient, outflow volumes are always lower for G_- than for G_+. The effect of the gradient is generally stronger when the rainstorm is of low intensity and short duration.

In order to better quantify the respective importance of each type of variability (stochastic or deterministic) in the variation of outflow volumes, the following ratios are used:

$$W_+ = \frac{\overline{V}_{(G_+,C_v\neq0)} - \overline{V}_{(G_0,C_v\neq0)}}{\overline{V}_{(G_0,C_v\neq0)} - V_{(G_0,C_v=0)}} \text{ and } W_- = \frac{\overline{V}_{(G_-,C_v\neq0)} - \overline{V}_{(G_0,C_v\neq0)}}{\overline{V}_{(G_0,C_v\neq0)} - V_{(G_0,C_v=0)}} \quad (13)$$

where the numerators and denominators reflect the effects of the variability of the deterministic and stochastic variabilities respectively.

Let $\sigma_s = C_v \times 12{\cdot}6$ mm h^{-1} be the standard deviation corresponding to the stochastic variation coefficient C_v and the global K_s mean. Let σ_d be the standard deviation in the pure deterministic (G_+, $C_v = 0$) or (G_-, $C_v = 0$) K_s maps. The standard deviation ratio σ_d/σ_s measures the relative magnitude of the two sources of K_s spatial variability (deterministic or stochastic) for a given set of K_s parameters (gradient G and coefficient C_v).

For selected storms (T^* and K^* coordinates), Figure 9 presents the W_+ and W_- ratios of Equation (13) as a function of σ_d/σ_s. As shown by Figure 9, the effect of a G_- gradient is always small compared with that of any stochastic K_s variability, whereas the relative effect of a G_+ gradient may be very large for events of low duration or intensity, i.e. those producing little runoff. For these events, runoff mostly originates from the low-permeability areas of the basin, and therefore strongly depends on the upslope–downslope distribution of K_s, i.e. on the possibility for downstream run-on infiltration. On the other hand, for storms producing significant runoff, i.e. with high duration and intensity, the G_+ effect (W_+) scales with the σ_d/σ_s ratio, and therefore remains small (much less than unity) for the smaller σ_d/σ_s values. When these are the events of major interest, it may be acceptable to ignore the deterministic K_s component for a σ_d/σ_s of 0·4 or below, which is a very common situation. The K_s variation coefficient of a homogeneous soil being generally considered close to unity (Nielsen *et al.*, 1973), σ_d/σ_s can be evaluated to around 0·2 in the Wankama catchment. The above simplification of the K_s spatial representation in this Sahelian environment may, therefore, be considered to model the significant runoff-producing events. However, as shown before, it is not acceptable to simplify further the K_s distribution to a uniform one, since the latter strongly underestimates outflows compared with a strictly stochastic distribution.

Peak discharge Q^*. The dimensionless peak discharge behaviour (Figure 10) is roughly similar to that of outflow volumes (Figure 7): Q^* tends towards unity when T^* increases or K^* decreases. However,

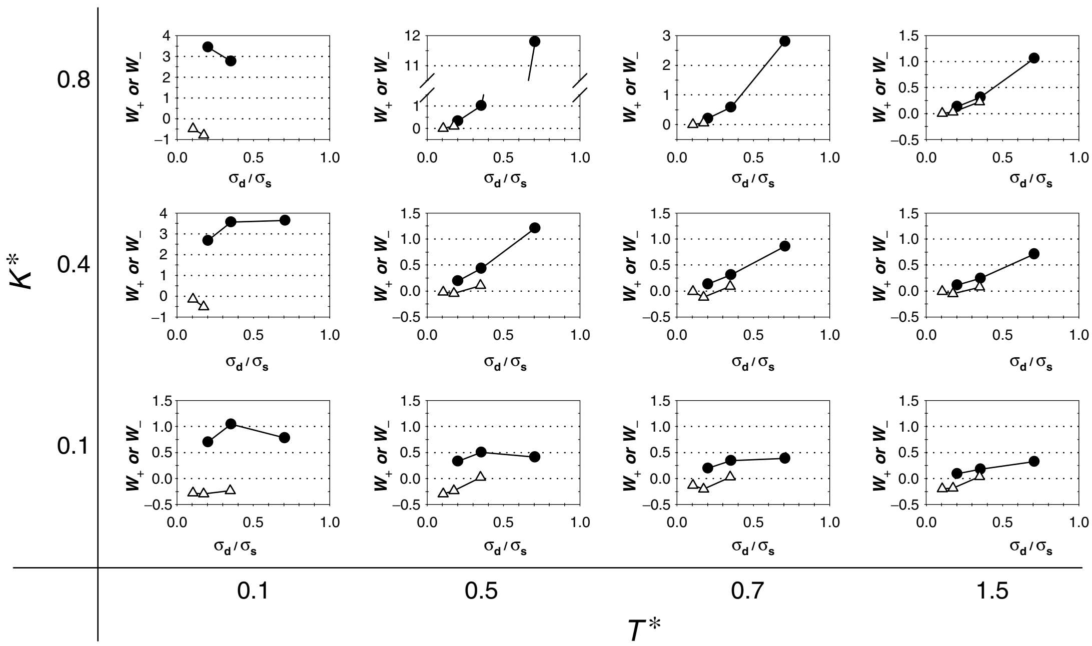

Figure 9. W_+ (●) and W_- (Δ) ratios [relative effects on outflow of deterministic and stochastic K_s variabilities, see Equation (13)] versus σ_d/σ_s, for various T^* and K^*

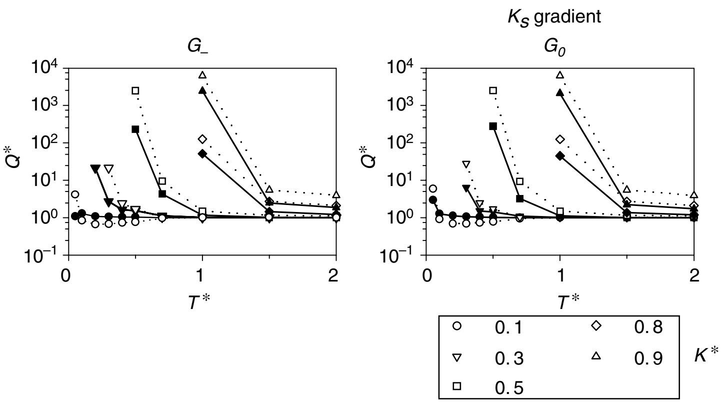

Figure 10. Dimensionless peak discharge Q^* versus K^*, K_s gradient, and C_v (filled symbol: $C_v = 0{\cdot}3$; unfilled symbol: $C_v = 1{\cdot}0$)

dimensionless peak discharge values are lower than dimensionless volumes, meaning that space heterogeneity has a smaller effect on peak discharge than on runoff volumes. This result was also pointed out by Saghafian *et al.* (1995) in the case of a basin with no K_s gradient. It appears to remain true for a non-zero gradient.

Figure 10 also shows that a small number of Q^* values are slightly lower than unity. They correspond to strong intensity (K^* equal to 0·1 and sometimes to 0·2 or 0·3) and short duration (T^* lower than unity). For these rainfall events, the increase in the variation coefficient results in a reduction in peak discharge (which in some cases is associated with a reduction in outflow volume). This is illustrated by an example in Figure 11 for a strictly stochastic K_s distribution (G_0). In Figure 11A, for a short, intense storm [$T^* = 0{\cdot}5$ (18 min) and $K^* = 0{\cdot}1$ (126 mm h^{-1})], the peak discharge tends to decrease when C_v increases. The more general, opposite behaviour is illustrated by Figure 11B for a longer, less intense event ($T^* = 1$ and $K^* = 0{\cdot}5$). An interpretation of Figure 11A may be that, for the short, intense events, infiltration on the most permeable grid-cells, whose K_s values increase with C_v, is a dominant runoff control factor.

Simulations with a drainage network

In order to mimic a typical Sahelian channel better, the drainage network (Figure 1) is assigned values of $K_s = 150$ mm h^{-1} and $n = 0{\cdot}03$, representative of a small, clean sandy bed. New simulations were run with this configuration, for the same initial moisture (5%) and rainstorm set, with the purely deterministic (G_+, G_-) and uniform (G_0) K_s distributions. As expected, all outflow volumes were found to decrease when a permeable network is introduced. Figure 12 compares the values, respectively with and without the permeable network, of the V^* ratio, which measures the effect of the G_+ or G_- gradient relatively to the G_0 reference. It appears that this effect is changed significantly by the channel type: a permeable channel increases V^* in

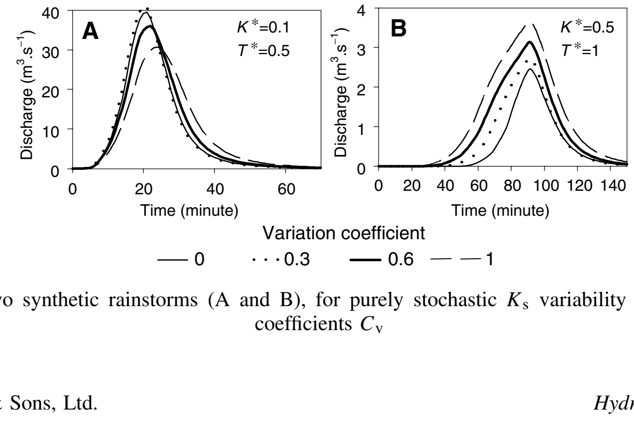

Figure 11. Hydrographs from two synthetic rainstorms (A and B), for purely stochastic K_s variability (G_0 case) with various variation coefficients C_v

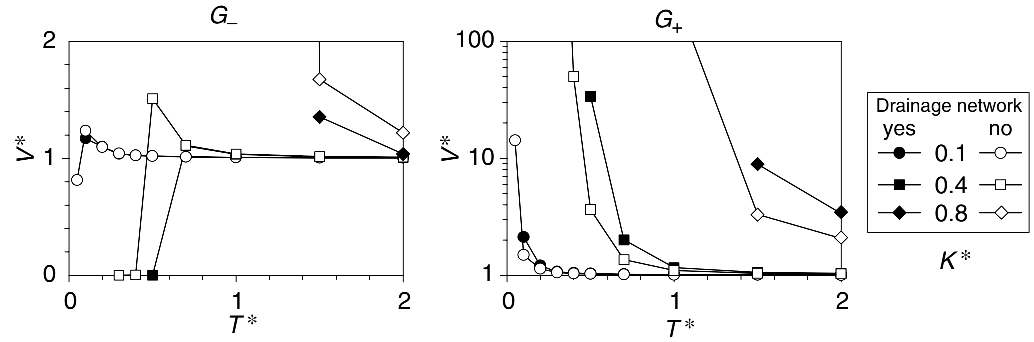

Figure 12. Dimensionless outflow volume V^* versus T^* and K^* with and without drainage network, for purely deterministic K_s distributions (positive G_+ and negative G_- gradient)

the G_+ case and lowers it in the G_- case. Indeed, in the G_+ case, the most impermeable, runoff-producing areas are located downhill, resulting in a lesser outflow reduction impact of the pervious channel than for the uniform K_s situation (G_0): the ratio $V^* = V_{G_+}/V_{G_0}$ is increased by the permeable channel, which therefore strengthens the runoff-boosting effect ($V^* > 1$) of the G_+ gradient relatively to G_0. Conversely, in the G_- case, the permeable channel amplifies the process of absorption of run-on from the more productive upper areas, thereby reducing V^* values. The effect of the G_- gradient relatively to G_0 is therefore intensified for short, intense events ($V^* < 1$) and lessened for longer, less intense events ($V^* > 1$).

The combination of stochastic K_s variability with a permeable drainage network is investigated in the section Simulations with actual rainstorms and K_s and n distributions.

Influence of initial degree of saturation

Simulations for the G_+, G_0 and G_- gradients and for C_v values equal to 0 and 0·3 are now run with a 95% uniform initial degree of saturation. Compared with the 5% saturation case, all runoff volumes are increased and become less sensitive to soil characteristics. This is illustrated in Figure 13 for the (G_+, $C_v = 0{\cdot}3$) case: for given values of T^* and K^*, V^* is much closer to unity for 95% saturation than for 5%. The effect of initial degree of saturation is to be paralleled with the previously described effect of rainfall duration T^*: when

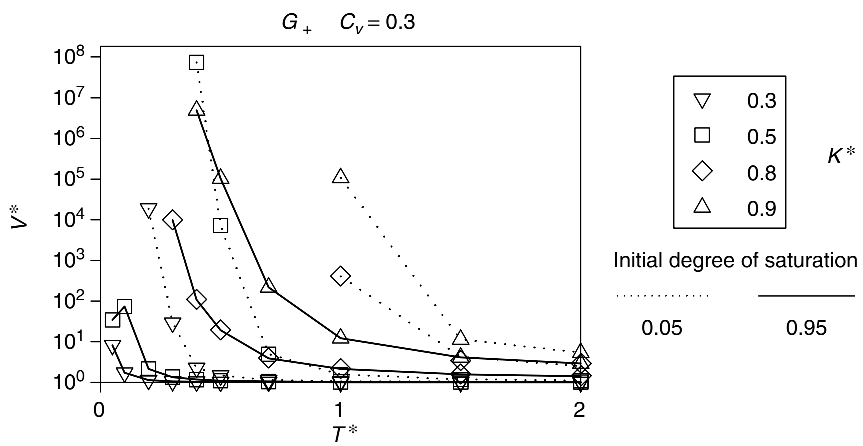

Figure 13. Dimensionless outflow volume V^* versus T^*, K^* and initial soil saturation, for a stochastic-deterministic K_s distribution (positive gradient G_+, $C_v = 0{\cdot}3$)

either one increases, actual infiltration rates get closer to the saturated hydraulic conductivity K_s values for a growing fraction of the event duration, leading to less effective infiltrability contrasts between the various distributions.

Simulations with actual rainstorms and K_s and n distributions

All results presented above refer to simulations with (i) synthetic, uniform rainstorms and (ii) theoretical log-normal distributions of K_s and n over the basin. Simulations are now made with the 15 actual rainstorms observed during the 1998 rainy season. The shortest interstorm duration was 3 days, so a 5% initial degree of saturation can reasonably be used for all storm simulations. Eight K_s (and n) distributions are considered in these simulations, consisting of the cross-combinations of four different hillslope parameter distributions and of two possible channel network configurations. The four hillslope distributions respectively consist of:

- the original K_s and n maps produced from SPOT images (this K_s distribution corresponds to the G_+ case, see Figure 2);
- the (G_0, $C_v = 0$) case: uniform K_s and roughness n;
- the (G_0, $C_v = 0{\cdot}3$) case: strictly stochastic, log-normal distribution of average $K_s = 12{\cdot}6$ mm h^{-1} and variation coefficient $C_v = 0{\cdot}3$, and derived n;
- the (G_0, $C_v = 1{\cdot}0$) case: same as above with increased variability.

The two channel alternatives are:

- the above rules are extended to the channel network;
- the specific channel values of $K_s = 150$ mm h^{-1} and $n = 0{\cdot}03$ (pervious network) are applied.

Figure 14 shows the seasonal runoff coefficient (ratio of total runoff over total rainfall) obtained with these eight scenarios. Whether or not the permeable network is included, the seasonal runoff coefficient obtained with the original K_s map is best predicted with a strictly stochastic distribution of K_s ($C_v = 0{\cdot}3$ or $0{\cdot}1$), rather than with a uniform K_s over the catchment.

The ranking of simulated runoff coefficients with respect to the K_s spatial distributions in Figure 14 is consistent with the previous simulation results. However, on a seasonal scale, with or without a permeable channel, the differences obtained between these runoff coefficients remain relatively low: it is only ±3% between the log-normal and the original K_s distribution and −7% between the uniform and the original K_s distributions. Hence, a uniform average K_s may be considered as a reasonable approximation for the seasonal water yield; an even better one is obtained by the introduction of a purely stochastic component. If a markedly more permeable channel exists, it is important to represent it explicitly.

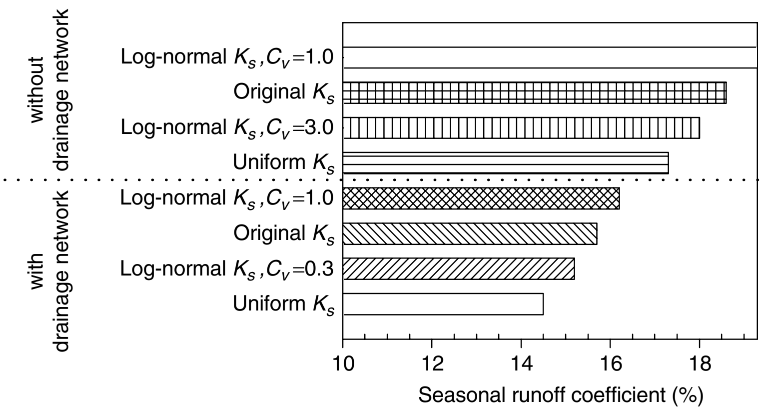

Figure 14. Runoff coefficient over the 1998 rainy season for different spatial distributions of K_s

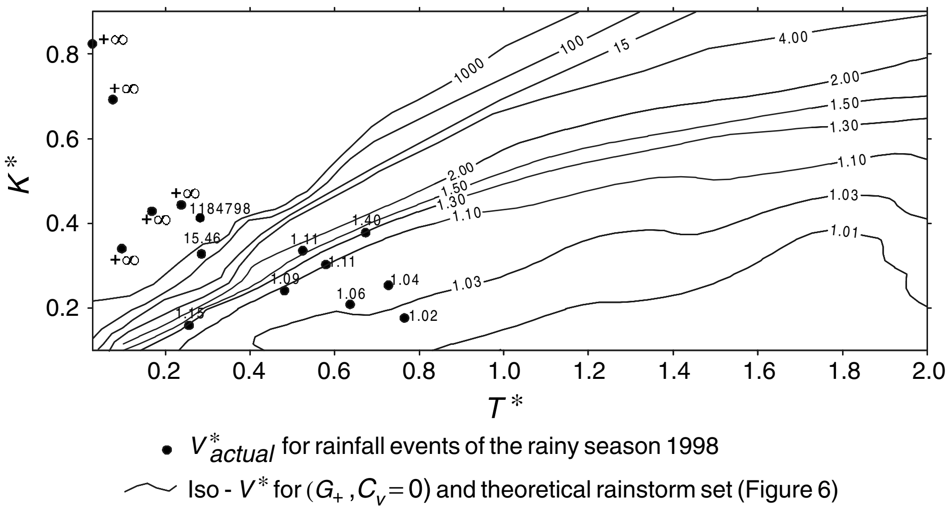

Figure 15. Plot in (T^*, K^*) rainfall space of actual 1988 rainstorms tagged with dimensionless outflow V^*_{actual} (computed with original K_s map) and of V^* isolines [dimensionless outflow for (G_+, $C_v = 0$) distribution of K_s and synthetic rainstorms)

To analyse at the event scale the results obtained with the actual data, the dimensionless parameters K^* and T^* are adapted to actual events (Séguis *et al.*, 1999). To compute T^*, the actual hyetographs are restricted to the intensities above the 12·6 mm h^{-1} threshold. K^* is computed for the average intensity during the reduced hydrograph. Simulations are performed with the original, actual hyetographs, K^* and T^* only being used for graphical representation. The dimensionless outflow volume V^*_{actual} is computed for each event as the ratio of the volume obtained with the original K_s map (no permeable channel) to the volume obtained for the uniform distribution. The (T^*, K^*) pairs relative to the rainfall events of 1998 are plotted in Figure 15, each point being labelled with the value of V^*_{actual}. To allow comparison with the case of a (G_+, $C_v = 0$) distribution, the background of Figure 15 presents, in the T^*–K^* space, the isolines of the V^* values of Figure 6. In accordance with the theoretical case, Figure 15 shows that V^*_{actual} is close to unity when K^* is low and T^* is high, i.e. when runoff is great. For low T^*, there is little or no runoff for uniform K_s, and V^* increases to infinity. These sharp differences for short storms are hidden in the seasonal total by the contributions from the more productive, longer events. Unlike modelling for the seasonal water yield, working at the event scale requires careful consideration of the type of spatial distribution of the basin's hydraulic characteristics (K_s and Manning n), as well as of those of the channel, especially for the smaller events.

DISCUSSION AND CONCLUSION

Using a Monte Carlo methodology together with the fully distributed hydrological model *r.water.fea*, we have investigated the influences on basin outflow of various spatial distributions of the hydraulic conductivity and roughness, the latter being totally conditioned by the former, for a small, semi-arid basin with exclusively Hortonian runoff. In addition to a uniform distribution of K_s (and therefore of n) used as a reference, strictly deterministic spatial distributions were first tested, where K_s is linearly dependent on elevation (positive or negative gradient). Then, a stochastic component was added to these distributions by a log-normal representation of K_s values with increasing coefficients of variation. The main results of the study are as follows.

1. Whatever the K_s gradient and/or stochastic variation coefficient, outflow volumes and peak discharges tend towards those calculated with a uniform K_s value when the storm is long and intense (low K^* and high T^*).

This is consistent with the result of Saghafian *et al*. (1995). The initiation time for a stochastic-deterministic K_s distribution is always shorter than for a uniform K_s distribution, all the more so as the stochastic variation coefficient increases; this behaviour is more pronounced when the rainfall intensity decreases. For most rainstorms, increasing the stochastic variation coefficient induces a runoff increase (outflow volume and peak discharge): a few exceptions to this general behaviour are found for intense and short rainfall events (K^* and T^* low), regarding peak discharge essentially.

2. Whatever the rainstorm and variation coefficient, the basin production is higher when K_s increases with elevation than when it decreases.
3. For significant runoff-producing events (high intensity and duration), the effect of the K_s gradient on outflow declines when the ratio of the deterministic to the stochastic standard deviation of K_s over the basin decreases. It reflects the fact that the variability of the hydrologic properties induced by the elevation is masked by the stochastic variability when the latter is high over the whole basin. For the Sahelian environment studied in this paper, this ratio is low, estimated around 0·2. It can be concluded that the effect of the deterministic component is small compared with the effect of the stochastic variability, for such events.

All these conclusions remain basically valid for a basin with a permeable channel. The permeable channel amplifies the effects on runoff volumes of the slopewise-deterministic K_s gradient, except in the case of long rainfall events of low intensity for a G_- gradient.

A number of consequences and practical implications can be inferred from these results. The first one is that, for many practical purposes, the representation of K_s distributions in Hortonian runoff models may be reasonably simplified as long as the natural, small-scale stochastic variability is accounted for. This is the case when the events of interest are those producing significant runoff. In semi-distributed models, for instance, it is desirable that K_s be described as a log-normal random variable by its mean and variation coefficient over each spatial model unit, instead of a single uniform value. Uniform distributions appear to underestimate the volumes. However, the effect of the hydrologic property distribution appears to be attenuated when considering the total seasonal water yield instead of that of a single event. Using a simplified, uniform distribution could be a reasonable choice as long as only a seasonal water resource estimate is required, at least in catchments where annual water yield is mostly obtained from large runoff-producing storm events.

Another implication for model calibration concerns the rainfall sample to be considered. The simulations showed that the hydrological model is more sensitive to K_s and n distributions when the rainfall event is short and/or of low intensity. Consequently, it may be appropriate to give greater weight to such events in a calibration sample.

ACKNOWLEDGEMENTS

We thank the anonymous reviewers for their valuable comments that helped to improve this paper.

REFERENCES

Albergel J, Ribstein P, Valentin C. 1986. L'infiltration: Quels facteurs explicatifs? Analyse des résultats acquis sur 48 parcelles soumises à des simulations de pluies au Burkina Faso. In *Journées hydrologiques de l'Orstom à Montpellier*, 17–18 September 1985, Orstom: Paris; 24–48.

Anderson SH, Cassel DK. 1986. Statistical and autoregressive analysis of soil physical properties of Portsmouth Sandy Loam. *Soil Science Society of America Journal* **50**: 1096–1104.

Boivin P, Touma J, Zante P. 1987. Mesure de l'infiltrabilité du sol par la méthode du double anneau. 1. Résultats expérimentaux. *Cahier ORSTOM, série Pédologie* **24**(1): 17–25.

Casenave A, Valentin C. 1992. A runoff capability classification based on surface features criteria in semi-arid areas of West Africa. *Journal of Hydrology* **130**: 231–249.

Chow VT. 1959. *Open Channel Hydraulics*. McGraw-Hill: New York; 685 pp.

Corradini C, Morbidelli R, Melone F. 1998. On the interaction between infiltration and Hortonian runoff. *Journal of Hydrology* **204**: 52–67.

Cuenca RH, Brouwer J, Chanzy A, Droogers P, Galle S, Gaze SR, Sicot M, Stricker H, Angulo Jaramillo R, Boyle SA, Bromley J, Chehbouni A, Cooper JD, Dixon AJ, Fiès JC, Gandah M, Gaudu JC, Laguerre L, Lecocq J, Soet M, Steward HJ, Vandervaere JP, Vauclin, M. 1997. Soil measurements during HAPEX–Sahel intensive observation period. *Journal of Hydrology* **188–189**: 224–266.

Desconnets JC, Vieux BE, Cappelaere B, Delclaux F. 1996. A GIS for hydrological modelling in the semi-arid, HAPEX–Sahel experiment of Niger, Africa. *Transaction in GIS* **1**(2): 82–94.

D'Herbès JM, Valentin C. 1997. Land surface conditions of the Niamey region: ecological and hydrological implications. *Journal of Hydrology* **188–189**: 18–42.

Duchaufour PH. 1984. *Abrégé de pédologie*. Masson: Paris; 220 pp.

Freeze RA. 1980. A stochastic-conceptual analysis of rainfall-runoff processes on a hillslope. *Water Resources Research* **16**(2): 391–408.

Hawkins RH, Cundy TW. 1987. Steady-state analysis of infiltration and overland flow for spatially-varied hillslopes. *Water Resources Research Bulletin* **23**(2): 251–255.

Hino M, Fujita K, Shutto H. 1987. A laboratory experiment on the role of grass for infiltration and runoff processes. *Journal of Hydrology* **90**(03–04): 303–325.

Hoogmoed WB, Strosnijder L. 1984. Crust formation on sandy soils in the Sahel. I.—Rainfall and infiltration. *Soil Tillage Research* **4**: 5–23.

Goutorbe JP, Lebel T, Tinga A, Bessemoulin P, Brouwer J, Dolman AJ, Engman ET, Gash JHC, Hoepffner M, Kabat P, Kerr YH, Monteny B, Prince S, Said F, Sellers P, Wallace JS. 1994. Hapex Sahel: a large scale study of land atmosphere interactions in the semi-arid tropics. *Annalae Geophysicae* **12**: 53–64.

Lamachère JM, Puech C. 1996. Cartographie des états de surface par télédétection et prédétermination des crues des petits bassins versants en zone sahélienne et tropicale sèche. In *L'hydrologie tropicale géoscience et outil pour le développement*, 2–4 May 1995, IAHS publ., no. 238; 235–248.

Le Barbé L, Lebel T. 1997. Rainfall climatology of the HAPEX–Sahel region during the years 1950–1990. *Journal of Hydrology* **188–189**: 43–73.

Loague K, Gander GA. 1990. R-5 revisited. 1. Spatial variability of infiltration on a small rangeland catchment. *Water Resources Research* **26**(5): 957–971.

Mein RG, Larson CL. 1973. Modeling infiltration during a steady rain. *Water Resources Research* **9**(2): 255–271.

Nielsen DR, Biggar JW, Erh KT. 1973. Spatial variability of field-measured soil-water properties. *Hilgardia* **42**: 215–259.

Peugeot C. 1995. *Influence de l'encroûtement superficiel du sol sur le fonctionnement hydrologique d'un versant sahélien (Niger). Expérimentation in-situ et modélisation*. Thesis, Université J. Fourier, Grenoble 1; 356.

Peugeot C, Esteves M, Galle S, Rajot JL, Vandervaere JP. 1997. Runoff generation, processes: results and analysis of field data collected at the East Central Supersite of the Hapex–Sahel experiment. *Journal of Hydrology* **188–189**(1–4): 179–202.

Rawls WJ, Brakensiek DL, Saxton KE. 1982. Estimation of soil water properties. *Transactions of the American Society of Agricultural Engineers* **25**(5): 1316–1320.

Saghafian B, Julien PY, Ogden FL. 1995. Similarity in catchment response 1. Stationary rainstorms. *Water Resources Research* **31**(6): 1533–1541.

Séguis L, Bader JC. 1997. Modélisation du ruissellement en relation avec l'évolution saisonnière de la végétation (mil, arachide, jachère) au centre Sénégal. *Revue des Sciences de l'Eau* **4**: 419–438.

Séguis L, Peugeot C, Cappelaere B, Maia-Bresson A. 1999. Simplifying a distributed, hydrological model for a semi-arid African environment. Effect of drainage topology. *Proceedings of AGU Spring Meeting, Hydrologic session: Scientific principles in distributed hydrologic process modeling: Is more complexity better?*, Boston, June.

Serpantié G, Tezenas du Moncel L, Valentin C. 1992. La dynamique des états de surface d'un territoire agropastoral soudano–sahélien. Conséquences et propositions. In *L'aridité: une contrainte au développement. Caractérisation, réponses biologiques*, ORSTOM: Paris; 419–447.

Smith RE, Hebert JN. 1979. A Monte Carlo analysis of the hydrologic effects of spatial variability of infiltration. *Water Resources Research* **15**(2): 419–429.

Thauvin V. 1992. *Étude de la répartition spatiale des précipitations en milieu sahélien à l'aide du réseau dense de pluviographes de l'expérience EPSAT–Niger: application à la détermination de la précision des moyennes surfaciques au pas de temps de l'événement pluvieux*. Thesis, Université de Montpellier 2; 229.

USACE. 1993. *GRASS 4·1 User's Reference Manual*. Construction Engineering Research Laboratories US Army Corps of Engineers: Champaign, Illinois.

Valentin C. 1986. Différencier les milieux selon leur aptitude au ruissellement: une cartographie adaptée aux besoins hydrologiques. In *Premières Journées hydrologiques de l'Orstom à Montpellier*, 17–18 September 1985, Orstom: Paris; 50–74.

Valentin C. 1991. Surface crusting in two alluvial soils of northern Niger. *Geoderma* **48**: 201–222.

Vandervaere J-P, Peugeot C, Vauclin M, Angulo Jaramillo R, Lebel T. 1997. Estimating hydraulic conductivity of crusted soils using disc infiltrometers and minitensiometers. *Journal of Hydrology* **188–189**: 203–223.

Vandervaere J-P, Vauclin M, Haverkamp R, Peugeot C, Thony J-L, Gilfedder M. 1998. Prediction of crust-induced surface runoff with disk infiltrometer data. *Soil Science* **163**(1): 9–21.

Vauclin M. 1982. Méthodes d'étude de la variabilité spatiale des propriétés d'un sol. In *Les colloques de l'INRA (15)*. INRA publ.: Paris; 9–43.

Vieux BE, Gaur N. 1994. Finite-element modeling of storm water runoff using GRASS GIS. *Microcomputers in Civil Engineering* **9**: 263–270.

Westervelt J (ed.). 1991. *GRASS Reference Manual, Version 4·0*. U.S. Army Construction Research Laboratory.

Woolhiser DA, Goodrich DC. 1988. Effects of storm rainfall intensity patterns on surface runoff. *Journal of Hydrology* **102**: 335–354.

Woolhiser DA, Smith RE, Giraldez JV. 1996. Effects of spatial variability of saturated hydraulic conductivity on Hortonian overland flow. *Water Resources Research* **32**(3): 9–43.

